Chapter 1
Ultrafast Laser Induced Confined Microexplosion: A New Route to Form Super-Dense Material Phases

Ludovic Rapp, Bianca Haberl, Jodie E. Bradby, Eugene G. Gamaly, Jim S. Williams and Andrei V. Rode

Abstract Intense ultrafast laser pulses tightly focused in the bulk of transparent material interact with matter in the condition where the conservation of mass is fulfilled. A strong shock wave generated in the interaction region expands into the surrounding cold material and compresses it, which may result in the formation of new states of matter. Here we show that the extreme conditions produced in the ultrafast laser driven micro-explosions can serve as a novel microscopic laboratory for high pressure and temperature studies well beyond the pressure levels achieved in a diamond anvil cell.

L. Rapp · A. V. Rode (✉) · E. G. Gamaly
Laser Physics Centre, Research School of Physics and Engineering, The Australian National University, Oliphant Building #60, Canberra ACT 0200, Australia
e-mail: avr111@physics.anu.edu.au

L. Rapp
e-mail: ludovic.rapp@anu.edu.au

E. G. Gamaly
e-mail: eugene.gamaly@anu.edu.au

B. Haberl · J. E. Bradby · J. S. Williams
Electronic Materials Engineering, Research School of Physics and Engineering, The Australian National University, Canberra ACT 0200, Australia
e-mail: bianca.haberl@anu.edu.au

J. E. Bradby
e-mail: jodie.bradby@anu.edu.au

J. S. Williams
e-mail: jodie.bradby@anu.edu.au

V. P. Veiko and V. I. Konov (eds.), *Fundamentals of Laser-Assisted Micro- and Nanotechnologies*, Springer Series in Materials Science 195,
DOI: 10.1007/978-3-319-05987-7_1,

1.1 Introduction

Ultrafast laser pulse at a μJ energy level tightly focused inside the bulk of a transparent solid can easily generate the MJ/cm^3 energy density, higher than the Young modulus of any solid, within a focal volume less than a cubic micron. The pressure of the order of several TPa (1 TPa = 10 Mbar) inside a focal volume leads to formation of a cavity (void) surrounded by a shell of compressed material. These two features of the phenomenon delineate two areas in the high-pressure material studies and their potential applications. The first area relates to the formation of different 3D structures, like photonic crystals, waveguides, and gratings etc. making use of multiple voids, separated or interconnected. For these studies the most important part is the process of void formation by a rarefaction wave following the shock wave. In order to produce a void one has to generate a pressure in excess of the strength (the modulus) of a material. The second area of research relates to the studies of material transformations under high pressure-temperature conditions, which are possible to create in tabletop laboratory experiments using powerful ultrafast laser pulses. The interaction of a laser with matter at the intensity above the ionisation and ablation threshold proceeds in a similar way for all the materials. The material converts into plasma in a few femtoseconds at the very beginning of the pulse, changing the interaction to the laser-plasma mode, increasing the absorption coefficient and reducing the absorption length, which ensures fast energy release in a very small volume. A strong shock wave generated in the interaction region propagates into the surrounding cold material. The shock wave propagation is accompanied by the compression of the solid material at the wave front and decompression behind it, leading to the formation of a void inside the material. The laser and shock wave affected material is in the shell that surrounds the void. This shell is the major object for studies of new phases and new material formation in strongly non-equilibrium conditions of confined microexplosion. Single pulse action thereby allows a formation of various three-dimensional structures inside a transparent solid in a controllable and predictable way.

First notion that the extreme conditions produced in the ultrafast laser driven confined micro-explosion may serve as a novel microscopic laboratory for high pressure and temperature studies, well beyond the levels achieved in diamond anvil cell, was presented by Glezer and Mazur in 1997 [1]. Recently it was experimentally demonstrated that it is possible to create super-high pressure and temperature conditions in table-top laboratory experiments with ultra-short laser pulses focused inside transparent material to the level significantly above the threshold for optical breakdown [2–4]. The laser energy absorbed in a sub-micron volume confined inside a bulk of pristine solid is fully converted into the internal energy. Therefore high energy density, several times higher than the strength of any material, can be achieved with ~100 fs, 1 μJ laser pulses focused down to a $1\,\mu m^3$ volume inside the solid.

Let us first to underline the differences between the intense laser-matter interaction at the surface of a solid and the case when laser-matter interaction is confined deep inside a solid by comparing the pressure created at the absorption region at the same intensity and total absorbed energy. At the intensity well over the ionisation

and ablation thresholds any material converts into plasma in a few fs time. Therefore the interaction proceeds most of the time in laser-plasma interaction mode. In these conditions the pressure at the ablated plume-solid interface (in laser-surface interaction) constitutes from the sum of thermal pressure of plasma next to the boundary plus the pressure from the recoil momentum of expanding plasma. Significant part of absorbed energy is spent on the expansion and heating of the ablated part of a solid. Therefore the ablation pressure in the case of surface interaction depends on the absorbed intensity by the power law $P_{abl} \propto I_{abs}^{m}; m < 1$. Alternatively, there is no expansion loss in confined interaction. Hence the maximum pressure is proportional to the absorbed intensity $P_{conf} \propto I_{abs}$ and it is almost twice larger than in the surface interaction mode.

Full description of the laser-matter interaction process and laser-induced material modification from the first principles embraces the self-consistent set of equations that includes the Maxwell's equations for the laser field coupling with matter, complemented with the equations describing the evolution of energy distribution functions for electrons and phonons (ions) and the ionisation state. A resolution of such a system of equations is a formidable task even for modern supercomputers. Therefore, the thorough analytical aprouch is needed. We split below this complicated problem into a sequence of simpler interconnected problems: the absorption of laser light, the ionisation and energy transfer from electrons to ions, the heat conduction, and hydrodynamic expansion.

1.2 Energy Density in Confined Ultra-Short Laser Interaction with Solids

The sequence of processes in the ultrashort laser induced microexplosion schematically presented in Fig. 1.1. In the following section we consider the major mechanisms of laser absorption, ionisation, and shock wave formation in confined geometry.

1.2.1 Absorbed Energy Density

Let us first define the range of laser and focussing parameters necessary for obtaining high pressure inside the interaction region. A 100 nJ laser pulse of duration $t_p \leq 100$ fs with the average intensity $I > 10^{14}$ W/cm^2 focussed into the area $S_{foc} \propto \lambda^2$ delivers the energy density >10 J/cm^2, well above the ionisation and ablation thresholds for any material [5]. The focal volume has a complicated three-dimensional structure. As a first approximation (that is also useful for scaling purposes) the focal volume is the focal area multiplied by the absorption length. The absorbed laser energy per unit time and per unit volume during the pulse reads:

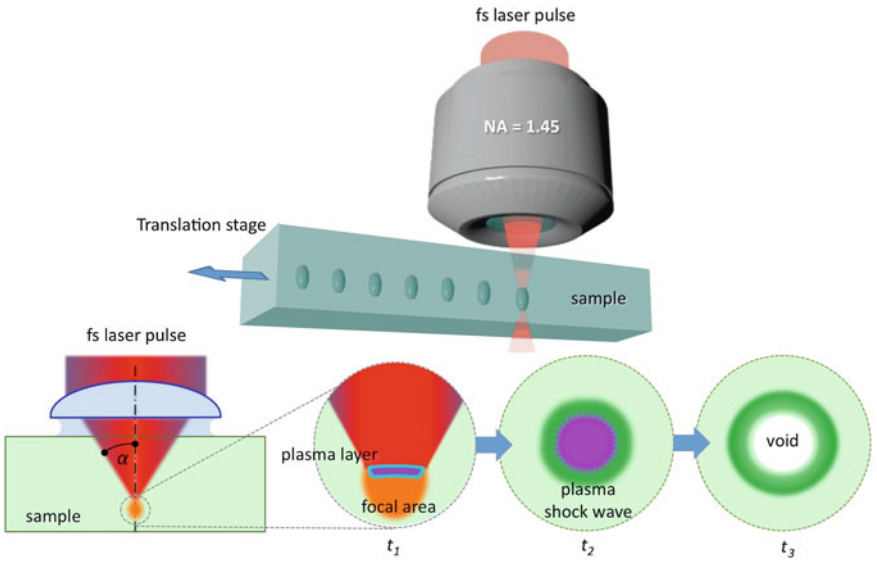

Fig. 1.1 Schematic representation of the experiments and the processes in fs-laser induced micro-explosion inside transparent dielectric. Three blown-up focal areas are shown in time sequences $t_1 < t_2 < t_3$. The first time slot t_1 during the pulse ~170 fs shows the formation of the energy absorbing plasma layer inside the focal area; the second interval $t_2 \sim 1$–100 ps shows hydrodynamic expansion of plasma and formation of a shock wave; the third $t_3 \sim 100$–1 ns shows rarefaction wave, and formation of a void surrounded by a densified shell due to quenching

$$\frac{\mathrm{d}E_{abs}}{\mathrm{d}t} = \frac{2A}{l_{abs}} I\,(r, z, t) \tag{1.1}$$

l_{abs} is the electric field absorption depth $l_{abs} = c/\omega k$. We assume that the electric field exponentially decays inside a focal volume, $E = E_0 \exp\{-x/l_{abs}\}$ as it does in the skin layer; A is the absorption coefficient defined by the Fresnel formula [6] as the following:

$$A = \frac{4n}{(n+1)^2 + k^2} = \frac{2\varepsilon''}{\left|1 + \varepsilon^{1/2}\right|^2 k}. \tag{1.2}$$

The duration of a typical short pulse of ~100 fs is shorter than the electron-phonon and electron-ion collision times. Therefore the electron energy distribution during the pulse has a delta function like shape peaked near the energy that can be estimated from the general formula of Joule heating (1.1) under the assumption that the spatial intensity distribution inside a solid, and material parameters are time independent. We denote the energy per single electron by ε_e (it should not be confused with the dielectric function that is always without a subscript here). Then the electron energy density change reads:

$$\frac{\mathrm{d}\,(n_e \varepsilon_e)}{\mathrm{d}t} = \frac{2A}{l_{abs}} I(t)\,. \tag{1.3}$$

We show later that the ionisation degree at $I > 10^{14}\,\mathrm{W/cm^2}$ is high, $Z > 1$, the number density of electrons is large, and electrons heat capacity can be taken as that for ideal gas. Thus from the above one can make a rough estimate of the electron temperature to the end of the pulse:

$$T_e \approx \frac{2A}{1.5 k_B\, n_e\, l_{abs}} I(t)\, t. \tag{1.4}$$

The electron temperature rises to tens of electron volts at the very beginning of the pulse. Fast ionisation of a solid occurs that affects absorption coefficient and absorption length. Thus, the next step is to introduce the model where the optical properties are dependent on the changing electron density and electron energy.

1.2.2 Ionisation Processes

Optical breakdown of dielectrics and optical damage produced by an intense laser beam has been extensively studied over several decades. Analytical estimates of the breakdown threshold, ionisation rates and transient number density of electrons created in the absorption region allows one to obtain the general picture of the processes in qualitative and quantitative agreement with computer simulations.

1.2.2.1 Ionisation Thresholds

It is generally accepted that the breakdown occurs when the number density of electrons in the conduction band reaches the critical density expressed through the frequency of the incident light by the familiar relation, $n_c = m_e\omega^2/4\pi e^2$. Thus, laser parameters, (intensity, wavelength, pulse duration) and material parameters (band-gap width and electron-phonon effective collision rate) at the breakdown threshold are combined by condition, $n_e = n_c$.

The ionisation threshold for the majority of transparent solids lies at intensities in between $(10^{13}$–$10^{14})\,\mathrm{W/cm^2}$ ($\lambda \sim 1\,\mu\mathrm{m}$) with a strong non-linear dependence on intensity. The conduction-band electrons gain energy in an intense short pulse much faster than they transfer energy to the lattice. Therefore the actual structural damage (breaking inter-atomic bonds) occurs after the electron-to-lattice energy transfer, usually after the end of the pulse. It was determined that in fused silica the ionisation threshold was reached to the end of 100 fs pulse at 1064 nm at the intensity $1.2 \times 10^{13}\,\mathrm{W/cm^2}$ [7]. Similar breakdown thresholds in a range of $(2.8 \pm 1) \times 10^{13}\,\mathrm{W/cm^2}$ were measured in interaction of 120 fs, 620 nm laser with glass, MgF_2, sapphire, and the fused silica [8]. This behaviour is to be expected, since all transparent dielectrics share the same general properties of slow thermal diffusion, fast electron-phonon scattering and similar ionisation rates. The breakdown threshold fluence ($\mathrm{J/cm^2}$) is an appropriate parameter for characterization conditions at different pulse duration.

It is found that the threshold fluence varies slowly if pulse duration is below 100 fs. For example, for the most studied case of fused silica the following threshold fluences were determined: ~2 J/cm^2 at 1053 nm; ~300 fs and ~1 J/cm^2 at 526 nm; ~200 fs [9]; 1.2 J/cm^2 (620 nm; ~120 fs) [8]; 2.25 J/cm^2 at 780 nm; ~220 fs [10, 11]; 3 J/cm^2 at 800 nm; 10–100 fs [12].

1.2.2.2 Ionisation Rates: Avalanche Ionisation

In interaction of lasers in a visible range with wide band gap dielectrics the direct photon absorption by electrons in a valence band is rather small. However, a few seed electrons can always be found in the conduction band. These electrons oscillate in the laser electromagnetic field and can be gradually accelerated to the energy in excess of the band-gap. Electrons with $\varepsilon_e > \Delta_{gap}$ collide with electrons in the valence band and can transfer them a sufficient energy to excite into the conduction band. Thus the number of free electrons increases, which provokes the effect of avalanche ionisation. The probability of such event per unit time (ionisation rate) can be estimated as follows:

$$w_{imp} \approx \frac{1}{\Delta_{gap}} \frac{\mathrm{d}\varepsilon_e}{\mathrm{d}t} = \frac{2\varepsilon_{osc}}{\Delta_{gap}} \frac{\omega^2 \nu_{eff}}{\left(\nu_{eff}^2 + \omega^2\right)}. \tag{1.5}$$

Electron is accelerated continuously in this classical approach. The oscillation energy is proportional to the laser intensity and to the square of the laser wavelength. At relatively low temperature corresponding to low intensities below the ablation threshold the effective collision rate, ν_{eff}, equals to the electron-phonon momentum exchange rate $\nu_{eff} = \nu_{e-ph}$. The electron-phonon momentum exchange rate increases in proportion to the temperature. For example, the electron-phonon momentum exchange rate in SiO_2 is of $\nu_{e-ph} = 5 \times 10^{14}\,\mathrm{s}^{-1}$[7] and it is lower of the laser frequency for visible light, $\omega \geq 10^{15}\,\mathrm{s}^{-1}$. Then the ionisation rate from (1.5) grows in proportion to the square of the laser wavelength in correspondence with the Monte-Carlo solutions to the Boltzmann kinetic equation for electrons [7]. With further increase in temperature and due to the ionisation, the effective collision rate becomes equal to the electron-ion momentum exchange rate, and reaches maximum approximately at the plasma frequency (~$10^{16}\,\mathrm{s}^{-1}$) [5, 13]. At this stage the wavelength dependence of the ionisation rate almost disappears due to $\omega < \nu_{e-i} \approx \omega_{pe}$, as it follows from (1.3) in agreement with rigorous calculations of [7]. In the beginning of the ionisation process, when $\omega > \nu_{e-ph}$, the ionisation rate is $w_{imp} \approx 2\nu_{e-ph} \sim 10^{14}$–$10^{15}\,\mathrm{s}^{-1}$. When the collision rate reaches its maximum, $\omega < \nu_{e-i} \approx \omega_{pe}$, the ionisation rate equals to $w_{imp} \approx 2\omega^2/\nu_{e-i} \approx 2\omega^2/\omega_{pe} \sim 5 \times 10^{14}\,\mathrm{s}^{-1}$.

1.2.2.3 Ionisation Rates: Multi-Photon Ionisation

Multiphoton ionisation has no intensity threshold and hence its contribution can be important even at relatively low intensity. Multi-photon ionisation creates the initial (seed) electron density, n_0, which then grows by the avalanche process. It proved to be a reasonable estimate of the ionisation probability (per atom, per second) in the multi-photon form [14]:

$$w_{mpi} \approx \omega n_{ph}^{3/2} \left(\frac{\varepsilon_{osc}}{2\Delta_{gap}} \right)^{n_{ph}}; \tag{1.6}$$

here $n_{ph} = \Delta_{gap}/\hbar\omega$ is the number of photons necessary for electron to be transferred from the valence to the conductivity band. The multi-photon ionisation process is important at low intensities as it generate the initial number of seed electrons, though small number, they are further multiplied by the avalanche process. The multi-photon ionisation rate dominates, $w_{mpi} > w_{imp}$, for any relationship between the frequency of the incident light and the effective collision frequency in conditions when $\varepsilon_{osc} > \Delta_{gap}$. However, even at high intensity the contribution of avalanche process is crucially important: at $w_{mpi} \sim w_{imp}$ the seed electrons are generated by multi-photon effect whilst final growth is due to the avalanche ionisation. Such an inter-play of two mechanisms has been demonstrated with the direct numerical solution of kinetic Fokker–Planck (1.14). Under the condition $\varepsilon_{osc} = \Delta_{gap}$, $\hbar\omega = 1.55$ eV, $n_{ph} = \Delta_{gap}/\hbar\omega \sim 6.4$, and $\omega = 2.356 \times 10^{15}\,\mathrm{s}^{-1}$, the multi-photon rate comprises $w_{mpi} \sim 5.95 \times 10^{15}\,\mathrm{s}^{-1}$. The ionisation time estimates as $t_{ion} \approx w_{mpi}^{-1}$. Thus, the critical density of electrons (the ionisation threshold) is reached in a few femtoseconds in the beginning of a 100-fs pulse. After that the interaction proceeds in a laser-plasma interaction mode.

1.2.2.4 Ionisation State During the Laser Pulse

In order to estimate the electron number density generated by the ionisation during the laser pulse the recombination processes should be taken into account. Electron recombination proceeds in dense plasma mainly by three-body Coulomb collisions with one of the electrons acting as a third body [15]. The cross section for the Coulomb collision reads $\sigma_{e-i} \approx \pi \left(e^2/\varepsilon_{el}\right)^2 Z^2$, while the probability for a third body (electron) presence in the vicinity of colliding particles is proportional to the cube of the Coulomb impact distance, $p_{3b} \propto r_{Coul}^3 = \left(e^2/\varepsilon_{el}\right)^3$. The growth rate of the electron number density is the balance of ionisation and recombination terms [4]:

$$\frac{\mathrm{d}n_e}{\mathrm{d}t} \approx n_e w_{ion} - \beta_e n_i n_e^2. \tag{1.7}$$

Here the ionisation rate is $w_{ion} = \max\left\{w_{mpi}, w_{imp}\right\} \sim 10^{15}\,\mathrm{s}^{-1}$, and the recombination rate is $\beta_e n_i n_e$, where the coefficient β_e is expressed as the following [15]:

$$\beta_e = 8.75 \times 10^{-27} \ln \Lambda Z^2 / \varepsilon_{el}^{9/2}. \tag{1.8}$$

We assumed that $n_e = Zn_i$, the electron energy ε_{el} is in eV; $\ln \Lambda$ is the Coulomb logarithm. One can see that ionisation time, $t_{ion} \approx w_{ion}^{-1}$, and recombination time $t_{rec} \approx (\beta_e n_i n_e)^{-1}$, are of the same order of magnitude, $\sim 10^{-15}$ s, and both are much shorter then the pulse duration. This is a clear indication of the ionisation equilibrium, and that the multiple ionisations $Z > 1$ take place. Therefore, the electron number density at the end of the pulse can be estimated in a stationary approximation as the follows: $n_e^2 \approx w_{ion}/Z\beta_e$. Taking $w_{ion} \sim 10^{15}\,\mathrm{s}^{-1}$; $\varepsilon_e \sim 30\,\mathrm{eV}$; $Z = 5$; $\ln\Lambda \sim 2$, one obtains, that number density of electrons at the end of the pulse becomes comparable to the atomic number density $n_e \sim 10^{23}\,\mathrm{cm}^{-3}$.

1.2.3 Increase in the Absorbed Energy Density Due to Modification of Optical Properties

We demonstrated above that the swift ionisation during the first femtoseconds in the beginning of the pulse produces the electron number density comparable to the critical density for the incident laser light, $n_e = n_c$. The free-electron number density grows up and becomes comparable to the ion density to the end of the pulse. Respectively, the electron-ion collision rate reaches its maximum that equals approximately to the plasma frequency in the dense non-ideal plasma. With further increase of electron temperature the electron-ion exchange rates decrease due to domination of the Coulomb collisions. The optical properties of this transient plasma are described by the Drude-like dielectric function; they are changing in accord with the change in electron density and temperature. Let us estimate the absorption coefficient and absorption length in the beginning of the laser pulse and at the end of the pulse. The dielectric function and refractive index in conditions, $\nu_{e-i} \approx \omega_{pe} \gg \omega$, are estimated as the following:

$$\varepsilon_{re} \approx \frac{\omega^2}{\omega_{pe}^2};\ \varepsilon_{im} \approx \frac{\omega_{pe}}{\omega};\ n \approx k = \left(\frac{\varepsilon_{im}}{2}\right)^{1/2}. \tag{1.9}$$

For example, after the optical breakdown of fused silica glass by 800 nm laser at high laser intensity ($\omega = 4.7 \times 10^{15}\,\mathrm{s}^{-1}$; $\omega_{pe} = 1.45 \times 10^{16}\,\mathrm{s}^{-1}$) the real and imaginary parts of refractive index are $n \sim k = 1.18$ thus giving the absorption length of $l_s = 54\,\mathrm{nm}$, and the absorption coefficient $A = 0.77$ [4]. Therefore, the optical breakdown and further ionisation and heating converts silica into a metal-like plasma medium reducing the energy deposition volume by up to two orders of magnitude when compared with the focal volume, and correspondingly massively increasing the

absorbed energy density and consequently the maximum pressure in the absorption region. For the interaction parameters presented above ($I = 10^{14}\,\mathrm{W/cm^2}$; $A = 0.77$; $l_s = 54\,\mathrm{nm}$; $t_p = 150\,\mathrm{fs}$) the pressure corresponding to the absorbed energy density equals to 4.4 TPa, ten times higher than the Young modulus of sapphire, one of the hardest of dielectrics. The general approach presented above is applicable for estimating parameters of any wide band gap dielectric affected by high intensity short pulse laser.

1.2.4 Energy Transfer From Electrons to Ions: Relaxation Processes After the Pulse

The hydrodynamic motion starts after the electrons transfer the absorbed energy to the ions. The following processes are responsible for the energy transfer from electrons to ions: recombination; electron-to-ion energy transfer in the Coulomb collisions; ion acceleration in the field of charge separation; electronic heat conduction. Below we compare the characteristic times of different relaxation processes.

1.2.4.1 Impact Ionisation and Recombination

The electron temperature in the energy units at the end of the pulse is much higher then the ionisation potential. Therefore, the ionisation by the electron impact continues after the pulse end. The evolution of the electron number density can be calculated in the frame of the familiar approach [15]:

$$\frac{\mathrm{d}n_e}{\mathrm{d}t} \approx \alpha_e n_e n_a - \beta_e n_i n_e^2; \tag{1.10}$$

here $\alpha_e = \sigma_e \nu_e n_e \,(I/T_e + 2)\exp(-I/T_e)\left[\mathrm{cm^3/s}\right]$ is the impact ionisation rate and β_e is the recombination rate connected to α_e by the principle of detailed balance. One can see that for parameters of experiments in question ($\sigma_e \sim 2 \times 10^{-16}\,\mathrm{cm^2}$; $\varepsilon_e \sim 30\,\mathrm{eV}$) the time for establishing the ionisation equilibrium is very short $\tau_{eq} \approx (\alpha_e n_e)^{-1} \sim 10^{-16}\,\mathrm{s}$. Thus the average charge of multiple ionised ions can be estimated from the equilibrium conditions using Saha equations. Losses for ionisation lead to temporary decrease in the electron temperature and in the total pressure [4]. However the fast recombination results in the increase in the ionic pressure.

1.2.4.2 Electron-to-Ion Energy Transfer by the Coulomb Collisions

The Coulomb forces dominate the interactions between the charged particles in the dense plasma created by the end of the pulse. The parameter that characterizes the plasma state is the number of particles in the Debye sphere, $N_D =$

$1.7 \times 10^9 \left(T_e^3/n_e\right)^{1/2}$ [16]. Plasma is in ideal state when $N_D \gg 1$. In the plasma with parameters estimated above for the fused silica ($Z = 5$, $\ln \Lambda = 1.7$; $n_e = 3 \times 10^{23}\,\mathrm{cm}^{-3}$; $\varepsilon_e = 50\,\mathrm{eV}$) N_D is of the order of unity, that is a clear signature of the non-ideal conditions. The maximum value for the electron-ion momentum exchange rate in non-ideal plasma approximately equals to the plasma frequency, $\nu_{ei} \approx \omega_{pe} \sim 3 \times 10^{16}\,\mathrm{s}^{-1}$ [13, 17, 18]. Hence electrons in ionised fused silica transfer the energy to ions over a time $t_{ei}^{en} \approx \left(\nu_{ei}^{en}\right)^{-1} \approx (M_i/m_e\nu_{ei}) \sim$(1–2) ps.

1.2.4.3 Ion Acceleration by the Gradient of the Electron Pressure

Let us estimate the time for the energy transfer from electrons to ions under the action of electronic pressure gradient when ions are initially cold. The Newton equation for ions reads:

$$\frac{\partial M_i n_i u_i}{\partial t} \approx -\frac{\partial P_e}{\partial x}$$

The kinetic velocity of ions then estimates as follows:

$$u_i \approx \frac{P_e}{M_i n_i \Delta x} t \tag{1.11}$$

The time for energy transfer from electrons to the ions is defined by condition that the ions kinetic energy compares to that of the electrons, $M_i u_i^2/2 \sim \varepsilon_e$. With the help of (1.11) one obtains the energy transfer time ($Z n_i \approx n_e$):

$$t_{el-st} \sim \frac{\Delta x}{Z} \left(\frac{\varepsilon_e}{2M_i}\right)^{-1/2}; \tag{1.12}$$

here $\Delta x \approx l_{abs} = 54\,\mathrm{nm}$ is the characteristic space scale. Then taking the time for the electron-to-ion energy transfer by the action of the electrostatic field of charge separation equals to $t_{el-st} \sim 1\,\mathrm{ps}$.

1.2.4.4 Electronic Heat Conduction

Energy transfer by non-linear electronic heat conduction starts immediately after the energy absorption. Therefore heat wave propagates outside of the heated area before the shock wave emerges. The thermal diffusion coefficient is defined conventionally as the following, $D = l_e v_e/3 = v_e^2/3\nu_{ei}$, where l_e, v_e and n_{ei} are the electron mean free path, the electron velocity and the momentum transfer rate respectively. The characteristic cooling time is conventionally defined as $t_{cool} = l_s^2/D$. For the conditions of experiments [2] $n_{ei} \sim \omega_{pe} \sim 3 \times 10^{16}\,\mathrm{s}^{-1}$; $\varepsilon_e = 50\,\mathrm{eV}$, and the cooling time is $t_{cool} = 3\omega_{pe} m_e l_{abs}^2/2\varepsilon_e = 14.9\,\mathrm{ps}$.

Summing up the results of the energy deposition in confined microexplosion we shall note that the major processes responsible for the electron-to-ion energy transfer in the dense plasma created by the tight focussing inside a bulk solid are different, and much shorter, when compared to those in the plume created by laser ablation. The ions acceleration by the gradient of the electronic pressure and the electron-to-ion energy transfer by the Coulomb collisions both comprise ~1 ps. The thermal ionization and recombination are in equilibrium, this permits the description of the plasma state by the Saha equations. The electronic non-linear heat conduction becomes important in the first ~15 ps after the pulse, and dominates the return to the ambient conditions.

1.3 Shock Wave Propagation and Void Formation

It was shown above that a focal volume as small as $0.2\,\mu m^3$ can be illuminated by focusing 800 nm laser pulses in the bulk of fused silica glass ($n = 1.453$) with a microscope objective with $NA = 1.35$ [2, 3]. The original focal volume shrinks to much smaller energy deposition region due to fast decrease in the absorption length, approximately five times less than the averaged focal radius. Modified shape of the absorption region has a complicated shape, which is practically unknown. Therefore, it is reasonable to assume for the further calculations that the absorption volume is a sphere of a smaller radius than the focal volume. One can see that 100 nJ of laser energy focussed in the volume of $0.2\,\mu m^3$ create the energy density of 5×10^5 J/cm^3 equivalent to the pressure of 0.5 TPa (5 Mbar). However this energy absorbs in much smaller volume thereby generating a pressure in excess of $P = 10$ TPa. All absorbed energy is confined in the electron component at the end of the 150-fs pulse.

1.3.1 Shock Wave Generation and Propagation

The hydrodynamic motion of atoms and ions starts when the electrons have transferred their energy to ions. This process is completed in a few picoseconds time, however one should note that the energy transfer time by the Coulomb collisions increases in proportion to the electron temperature. So, in solid-state density plasma formed in confined microexplosion the higher the absorbed energy, the longer the time for hydrodynamic motion to start. The pressure in a range of several TPa builds up after electron-ion energy equilibration; this pressure considerably exceeds the Young modulus for majority of materials. For example, the Young modulus for sapphire equals to 0.3–0.4 TPa, and that for silica is ~0.07 TPa. The high pressure generates the shock wave propagating from the energy absorption region into the surrounding cold material. The bulk modulus of the cold material equals to the cold pressure, P_c. This cold counter pressure finally decelerates and stops the shock wave. Because the shock driving pressure significantly exceeds the cold pressure, $P \gg P_c$, the strong shock emerges compressing a solid to the limit allowed by the equation

of state of a solid, which does not depend on the magnitude of the driving pressure. The maximum density of a perfect gas with the adiabatic constant γ is as the follows:

$$\rho = \frac{\gamma + 1}{\gamma - 1} \rho_{0_e}. \tag{1.13}$$

The adiabatic constant for a cold solid is conventionally estimates as $\gamma \sim 3$ [15]. Therefore maximum density after the shock front is expected to be $\rho_{\max} = 2\rho_0$. The compression ratio gradually decreases to unity along the shock propagation, deceleration and transformation into a sound wave. Note that the temperature in the compressed solid behind the shock front in the limit of $P \gg P_c$ grows in proportion to the driving pressure:

$$T = \left(\frac{\gamma - 1}{\gamma + 1}\right) \frac{P}{P_c} T_0 \tag{1.14}$$

Thus material is compressed and heated behind the shock wave front. Hence, the conditions for transformation to another phase might be created and this phase might be preserved after unloading to the normal pressure. The final state of matter may possess different properties from those in the initial state.

1.3.2 Shock Wave Dissipation

The shock wave propagating in a cold material loses its energy due to dissipation, e.g. due to the work done against the internal pressure (Young modulus) that resists material compression. The distance at which the shock wave effectively stops defines the shock-affected area. At the stopping point the shock wave converts into a sound wave, which propagates further into the material without inducing any permanent changes to a solid. The distance where the shock wave stops can be estimated from the condition that the internal energy in the whole volume enclosed by the shock front is comparable to the absorbed energy: $4\pi P_0 r_{stop}^3/3 \approx E_{abs}$ [15]. The stopping distance obtained from this condition reads:

$$r_{stop} \approx \left(\frac{3E_{abs}}{4\pi P_0}\right)^{1/3}. \tag{1.15}$$

In other words, at this point the pressure behind the shock front equals to the internal pressure of the cold material. One can reasonably suggest that the sharp boundary observed between the amorphous (laser-affected) and crystalline (pristine) sapphire in the experiments [2, 3] corresponds to the distance where the shock wave effectively stopped. The sound wave continues to propagate at $r > r_{stop}$ apparently not affecting the properties of material. For 100 nJ of absorbed energy and sapphire, taking $P_c = 0.4$ TPa for sapphire, one gets from (1.15) $r_{stop} = 180$ nm, which is in qualitative agreement with the experimental values.

1.3.3 Rarefaction Wave: Formation of Void

The experimentally observed formation of void, which is a hollow or low-density region, surrounded by a shell of the laser-affected material, can be qualitatively understood from the following simple reasoning. Let us consider for simplicity spherically symmetric explosion. The strong spherical shock wave starts to propagate outside the centre of symmetry of the absorbed energy region, compressing the material. At the same time, a rarefaction wave propagates to the centre of symmetry decreasing the density in the area of the energy deposition. This problem qualitatively resembles the familiar hydrodynamic phenomenon of strong point explosion ($P \gg P_0$) in homogeneous atmosphere with counter pressure taken into account. It is characteristic of a strong spherical explosion that material density decreases rapidly in space and time behind the shock front in direction to the centre of symmetry. Practically, the entire mass of material, initially uniformly distributed in the energy deposition region inside a sphere of radius $r \sim l_{abs}$, is concentrated within a thin shell near the shock front some time after the explosion. The temperature increases and density decreases towards the centre of symmetry, while the pressure is almost constant along the radius [15]. This picture is qualitatively similar to that observed in the experiments [4] as a result of fs-laser pulses tightly focussed inside sapphire, silica glass and polystyrene. A void surrounded by a shell of laser-modified material was formed at the focal spot. Hence, following the strong point explosion model, one can suggest that that the whole heated mass in the energy deposition region was expelled out of the centre of symmetry and was frozen after shock wave unloading in the form of a shell surrounding the void.

One can apply the mass conservation law for estimate of the density of compressed material from the void size measured in the experiment. Indeed, the mass conservation relates the size of the void to compression of the surrounding shell. We assume that in conditions of confinement no mass losses could occur. One can use the void size and size of the laser-affected material from the experiments and deduce the compression of the surrounding material. The void formation inside a solid only possible if the mass initially contained in the volume of the void was pushed out and compressed. Thus after the micro-explosion the whole mass initially confined in a volume with of radius r_{stop} resides in a layer in between r_{stop} and r_v, which has a density $\rho = \delta\rho_0$; $\delta > 1$:

$$\frac{4\pi}{3} r_{stop}^3 \rho_0 = \frac{4\pi}{3} \left(r_{stop}^3 - r_{void}^3 \right) \rho . \tag{1.16}$$

Now, the compression ratio can be expressed through the experimentally measured void radius, r_{void}, and the radius of laser-affected zone, r_{stop}, as follows:

$$r_{void} = r_{stop} \left(1 - \delta^{-1} \right)^{1/3} . \tag{1.17}$$

It was typically observed that $r_{void} \sim 0.5 r_{stop}$ in experiments of [4]. Applying (1.16), (1.17) one obtains that compressed material in a shell has a density 1.14 times higher than that of crystalline sapphire. Note that the void size was measured at the room temperature long after the interaction.

1.4 Density and Temperature in the Shock-Wave and Heat-Wave Affected Solid

1.4.1 Two Characteristic Areas in Confined Microexplosion

There are two distinctive regions in the area affected by laser action, which is confined inside a cold solid. First is the area where the laser energy is absorbed. Second area relates to the zone where shock wave propagates outside the absorption zone, compresses and heats the initially cold crystal and then decelerates into the sound wave, which apparently does not affect the pristine crystal. In the first area the crystal is heated to the temperature of tens of eV ($\sim 10^5$ K). It is swiftly ionised at the density close to that of a cold solid. In picosecond time the energy is transferred to ions and shock wave emerges. Conservatively, the heating rate estimates approximately as 10 eV/ps $\sim 10^{17}$ K/s. Then this material undergoes fast compression under the action of the micro-explosion and its density may increase to the maximum of $\sim$2 times the solid density. The energy dissipation in the shock wave and by the heat conduction takes nanoseconds. In the second zone heated and compressed exclusively by the shock wave the maximum temperature reaches several thousands Kelvin, approximately 10 times less than in the first zone. Heating and cooling rates in this zone are of the order of $\sim 10^{14}$ K/s.

Phase transformations in quartz, silica and glasses induced by strong shock waves have been studied for decades, see [15, 19] and references therein. However all these studies were performed in one-dimensional (plane) open geometry when unloading into air was always present. The pressure ranges for different phase transitions to occur under shock wave loading and unloading have been established experimentally and understood theoretically [19]. Quartz and silica converts to dense phase of stishovite (mass density 4.29 g/cm^3) in the pressure range between 15–46 GPa. The stishovite phase exists up to a pressure 77–110 GPa. Silica and stishovite melts at pressure $>$110 GPa that is in excess of the shear modulus for liquid silica $\sim$10 GPa. Dense phases usually transform into a low density phases (2.29–2.14 g/cm^3) when the pressure releases back to the ambient level. Numerous observations exist of amorphisation upon compression and decompression. An amorphous phase of silica denser than the initial state sometimes forms when unloading occurs from 15–46 GPa. Analysis of experiments shows that the pressure release and the reverse phase transition follows an isentropic path.

In the studies of shock compression and decompression under the action of shock waves induced by explosives or kJ-level ns lasers, the loading and release time scales

are in the order of ~1–10 ns [20–23]. The heating rate in the shock wave experiments is 10^3 K/ns = 10^{12} K/s, 5 orders of magnitude slower than in the confined micro-explosion.

In contrast, the peak pressure at the front of shock wave, driven by the laser in confined geometry, reaches the level of TPa, that is, 100 times in excess of pressure value necessary to induce structural phase changes and melting. Therefore, the region where the melting may occur is located very close to that where the energy is deposited. The zones where structural changes and amorphisation might occur are located further away. Super-cooling of the transient dense phases may occur if the quenching time is sufficiently short. Short heating and cooling time along with the small size of the area where the phase transition takes place can affect the rate of the direct and reverse phase transitions. In fact, phase transitions in these space and time scales have been studied very little.

The refractive index changes in a range of 0.05–0.45 along with protrusions surrounding the central void that were denser than silica were observed as a result of laser-induced micro-explosion in a bulk of silica [24]. This is the evidence of formation of a denser phase during the fast laser compression and quenching; however, little is known of the exact nature of the phase. Thus, we can conclude that a probable state of a laser-affected glass between the void and the shock stopping edge may contain amorphous or micro-crystallite material denser than the pristine structure and with a larger refractive index than the initial glass [24].

1.4.2 Upper Limit for the Pressure Achievable in Confined Interaction

The micro-explosion can be considered as a confined one if the shock wave affected zone is separated from the outer boundary of a crystal by the layer of pristine crystal m-times thicker than the size of this zone. On the other side the thickness of this layer should be equal to the distance at which the laser beam propagates without self-focussing L_{s-f} (W/W_c) [25]:

$$L_{s-f} = \frac{2\pi n_0 r_0^2}{\lambda}\left(\frac{W_0}{W_{cr}} - 1\right)^{-1/2} \tag{1.18}$$

W is the laser power, W_c is the critical power for self-focussing:

$$W_{cr} = \frac{\lambda^2}{2\pi\, n_0\, n_2} \tag{1.19}$$

This condition expresses as the following:

$$L_{s-f} = m r_{stop} \tag{1.20}$$

The absorbed energy, $E_{abs} = AE_{las}$, expressed through the laser power $W = E_{las}/t_p$ (E_{las}, t_p are respectively energy per pulse and pulse duration), and the radius of shock wave affected zone are connected by the equation:

$$r_{stop} \approx \left(\frac{3A\,W\,t_p}{4\pi P_{cold}}\right)^{1/3}. \tag{1.21}$$

The condition of (1.20) with (1.21) for the self-focusing length inserted then turns to the equation for the maximum laser power at which micro-explosion remains confined and self-focussing does not affect the crystal between the laser affected zone and outer boundary:

$$\frac{2n_0\pi r_0^2}{m\lambda}\left(\frac{4\pi P_{cold}}{3AW_c t_p}\right)^{1/3} = \left(\frac{W}{W_c}\right)^{1/3}\left(\frac{W}{W_c}-1\right)^{1/2}. \tag{1.22}$$

The left-hand side in (1.22) can be calculated if the laser pulse duration and focal spot area are both known. Taking, for example, sapphire ($n_0 = 1.75$); $W_c = 1.94\,\mathrm{MW}$; $\lambda = 800\,\mathrm{nm}$; $4\pi P_{cold}/3 = 1.67\,\mathrm{MJ}$; $t_p = 100\,\mathrm{fs}$; $\pi r_0^2 = 0.2\,\mu\mathrm{m}^2$; $m = 3$, one gets 0.6 in the LHS of (1.22). Thus the maximum laser power allowed in these conditions equals to $\sim 1.3W_c = 2.5\,\mathrm{MW}$ or 250 nJ of the energy in 100 fs laser pulse. For conditions considered above the maximum pressure that can be achieved in absorption volume confined inside the transparent crystal might be up to 27 TPa, approximately three times higher that was achieved in the experiments [2].

1.4.3 Ionisation Wave Propagation Towards the Laser Beam

There is an additional effect in the focal zone which can influence the size of the volume absorbing the laser energy at the laser fluence above the optical breakdown threshold F_{thr}, namely, the motion of ionisation front with critical density in the direction towards the laser beam propagation. It was first discovered in studies of optical breakdown in gases [14]. Indeed, the intense beam with the total energy well above the ionisation threshold reaches the threshold value at the beginning of the pulse. Laser energy increases and the beam cross-section where the laser fluence is equal to the threshold value, the ionisation front, starts to move in the opposite to the beam direction. The beam is focussed to the focal spot area, $S_f = \pi r_f^2$. The spatial shape of the beam path is a truncated cone, the intensity at any time to be independent of the transverse coordinates (see Fig. 1.2).

The ionisation time, i.e. the time required for generating the number of electrons to reach the critical density in the conduction band, is defined by (1.1). Therefore, the threshold fluence is achieved at the beam cross-section with a radius increasing as the following:

$$r\,(z,t) = r_f + z\,(t)\,tg\alpha \tag{1.23}$$

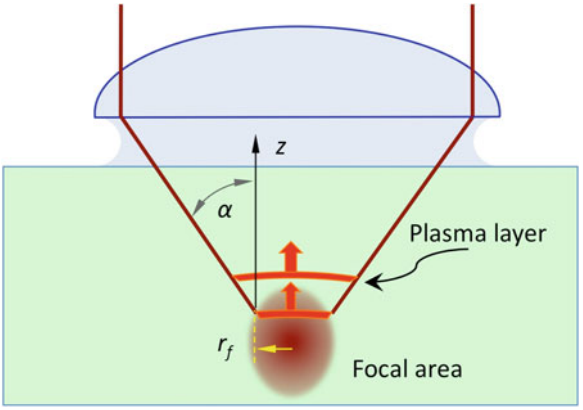

Fig. 1.2 The path of the converging focused pulse as a truncated cone. The motion of the ionisation front toward the beam propagation is indicated by the *red arrows*

where, z is the distance from the focal spot, which is usually a circle with radius r_f. Then at any moment t during the pulse the relation holds:

$$\frac{E_{las}(t)}{\pi r^2(z,t)} = F_{thr} \tag{1.24}$$

We introduce the dimensionless parameter, $f = E_{las}(t_p)/\pi r_f^2 F_{thr} = F_{las}/F_{thr}$, as the ratio of the maximum fluence to the threshold fluence. Then the ionisation front moved the distance z(t_p):

$$z(t_p) = \frac{r_f}{tg\alpha}\left(f^{1/2} - 1\right). \tag{1.25}$$

Correspondingly, the ionisation time can be evaluated as:

$$t_{ion} = t_p\left[1 - \left(1 - \frac{1}{f}\right)^{1/2}\right]. \tag{1.26}$$

One can see that if the total fluence equals to that for the threshold, $f = 1$, the n_{cr} is reached only at the end of the pulse [9, 26, 27], the ionisation time equals to the pulse duration and thus there is no movement of the ionisation front. These simple geometrical considerations are in qualitative agreement with the experiments in sapphire and silica. Indeed, the voids measured in sapphire and in silica in the references [2–4] are slightly elongated; the (1.25) gives $z_m = 0.67r_f$ and $z_m = 0.45r_f$ for sapphire and silica respectively.

Summing up the results of this section, the effects of the blue shift of the pulse spectrum and the intensity dependence of the group velocity are small and rather

positive for achieving high absorbed energy density. The negative effect of the ionisation front motion at the laser energy well above the ionisation threshold leads to a large decrease in the absorbed energy density. The negative effect of defocusing needs further careful studies with the solution of Maxwell equations.

1.4.4 Modelling of Macroscopic Explosions by Micro-Explosion

The micro-explosion process can be described solely in the frames of the ideal hydrodynamics if the heat conduction and other dissipative processes, all characterized by specific length scales, could be ignored. The hydrodynamic equations contain five variables: the pressure, P, the velocity, v, the density, ρ, the distance, r, and the time, t. The last three of them are independent parameters, and the other two can be expressed through the previous three. The micro-explosion can be fully characterized by the following independent parameters: the radius of the energy deposition zone, R_0, the total absorbed energy, E_0, and the initial density ρ_0. Then the initial pressure, $P_0 = E_0/R_0^3$, and the initial velocity, $v_0 = (P_0/\rho_0)^{1/2}$ are combinations of the independent parameters. One can neglect the energy deposition time and time for the energy transfer from electrons to ions (picosecond) in comparison to hydrodynamic time of a few nanoseconds. Then, the hydrodynamic equations can be reduced to the set of the ordinary equations with one variable [15], $\xi = r/v_0 t$, describing any hydrodynamic phenomena with the same initial pressure and density (velocity), but with the characteristic distance and time scales changed in the same proportion. When the energy of explosion increases, the space, R_0, and time scales are increased accordingly to $R_0 = (E_0/p_0)^{1/3}$; $t_0 = R_0/v_0$. The similarity laws of hydrodynamics in micro- and macroscopic explosions suggest that micro-explosion in sapphire ($E_0 = 10^{-7}$ J; $\rho_0 \sim 4\,\mathrm{g/cm^3}$; $R_0 = 1.5 \times 10^{-5}$ cm; $t_0 = 5.5 \times 10^{-12}$ s) is a reduced copy of macroscopic explosion that produces the same pressure at the same initial density but with the energy deposition area size and time scales changed in accordance with the above formulae. For example, the energy of 10^{14} J (that is equivalent to 25,000 tons of high explosive or one nuclear bomb) released in a volume of 4 cubic meters ($R_0 = 1.59$ m) during the time of 20 μs exerts the same pressure of 12.5 TPa as the laser-induced micro-explosion in sapphire does. Thus, exactly the same physical phenomena occur at the scale 10^7 times different in space and in time, and 10^{21} times different in energy. Therefore, all major hydrodynamic aspects of powerful macroscopic explosion can be reproduced in the laboratory tabletop experiments with ultra-short laser pulses.

1.5 Formation of Void at Si/SiO_2 Interface

The experiments were conducted with 170 fs, 790 nm, laser pulses from a MXR-2001 CLARK laser system. Pulses with up to 2.5 μJ per pulse were focused using an optical microscope (Olympus IX70) equipped with an oil-immersion ×150 objective (NA = 1.45) The focal spots were measured using a knife-edge technique with a sharp edge of a Si(100) wafer etched at 54.74° to the surface along the (111) direction and mounted on a nano-positioning stage. The focal spots were measured to have a radius of 0.368 μm at the full-width at half-maximum level. The experiments were conducted with laser pulses at 1 kHz repetition rate in a sample moved at a rate 2 mm s^{-1} to guarantee a single shot per spot regime, so that each of the shots was located 2 μm apart.

Silicon is not transparent for 790 nm, the wavelength that we used for the experiments. While the laser induced micro-explosion method was previously considered as suitable only for transparent materials, we propose to expand it into the unexplored domain of non-transparent materials. To confine laser-matter interaction inside a material the distance ought to be far enough from the crystal surface in order the interaction region can be considered as confined. The interaction of intense laser radiation with matter when the beam is tightly focused inside a transparent material is radically different from the case of focusing the beam onto a surface. In the laser-surface interaction the temperature has maximum at the outermost atomic surface layer. If the absorbed energy density in the surface layer is in excess of ablation threshold, the atomic bonding breaks and the ablated atoms leave the surface. In tightly focused interaction mode the focal zone with high energy density is confined inside a bulk of a cold and dense solid. The laser-affected material remains at the focal area inside the pristine material.

By growing a transparent oxide on the sample, laser induced confined micro-explosion can be applied to virtually any opaque material. The confinement conditions were formed in silicon wafers covered by 10-μm thick layer of dioxide of silicon (SiO_2). SiO_2 is transparent to the laser irradiation and allow tightly focusing femtosecond laser pulses on the buried surface of the Si crystal. The thickness of the SiO_2 layer was not so deep for developing large spherical aberrations with high-NA focusing optics and at the same time guarantee the absence of optical breakdown at the surface.

Silicon crystal was exposed to strong shock wave induced by fs-laser micro-explosion in confined geometry [18]. Figure 1.1 shows a schematic representation of the process and the realization of array of voids using focusing fs-pulses at the Si/SiO_2 interface. After processing the array have been investigated by optical microscopy. Figure 1.3 presents an optical microscope image of a top-view of the sample of the laser-affected areas at the Si/SiO_2 interface. The dark dots in the picture are the voids. The voids were spaced from 2 μm. The voids are observed through the SiO_2 layer.

To analyse the dimensions of the voids and of the shock wave modified areas, we opened the sample using a focused ion beam (FIB) technique. The sample was gold coated by sputtering (5 nm). The layer of SiO_2 was removed, as shown on Fig. 1.4a, and then the sample was characterized with scanning electron microscopy (SEM).

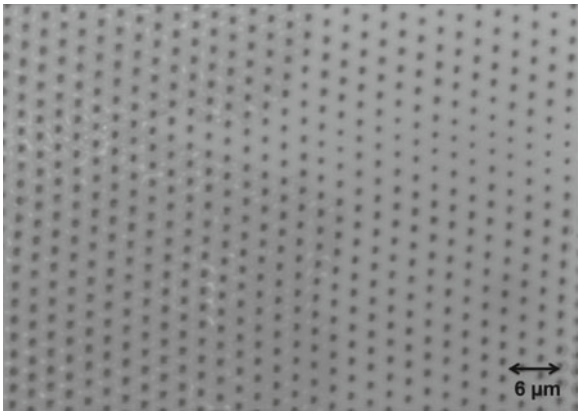

Fig. 1.3 Optical microscope image of arrays of void made at Si/SiO_2 interface viewed through the SiO_2 layer produced fs-pulse laser micro-explosion. The spacing between the void is 2 µm

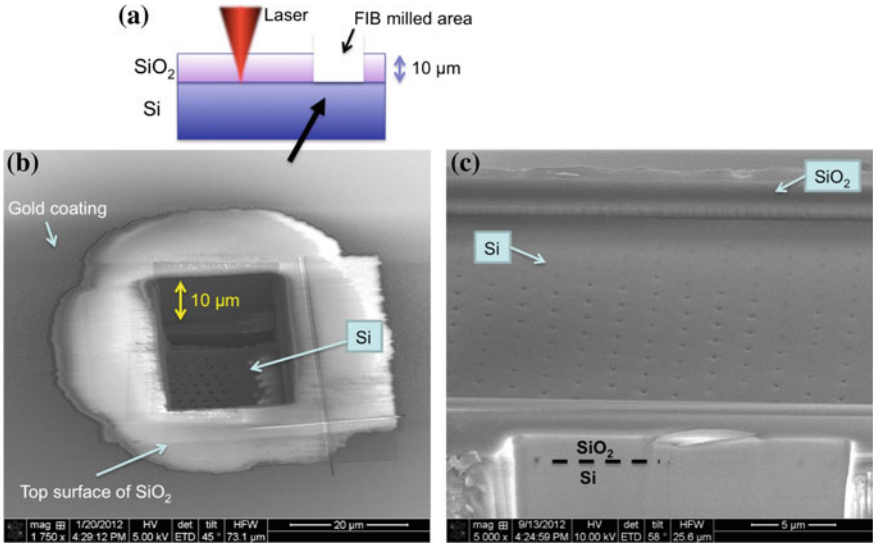

Fig. 1.4 **a** Side-view schematic representation of the processed sample and of the area milled using the focused ion beam (*FIB*). **b** SEM image of the hole made in the SiO_2 layer by FIB to reach the surface of the Si layer, following the schematic in (**a**). **c** SEM image of the side-view of the milling by FIB of the SiO_2 layer to reach the surface of the Si layer

Figure 1.4b presents a top-view SEM image of the sample where the 10 µm thick SiO_2 was removed where we can see the Si surface and arrays of voids. Voids were observed under the surface in the region where the fs-laser was focused. Figure 1.4c shows the Si surface and the arrays of voids; on the side-view we can observe the Si/SiO_2 boundary.

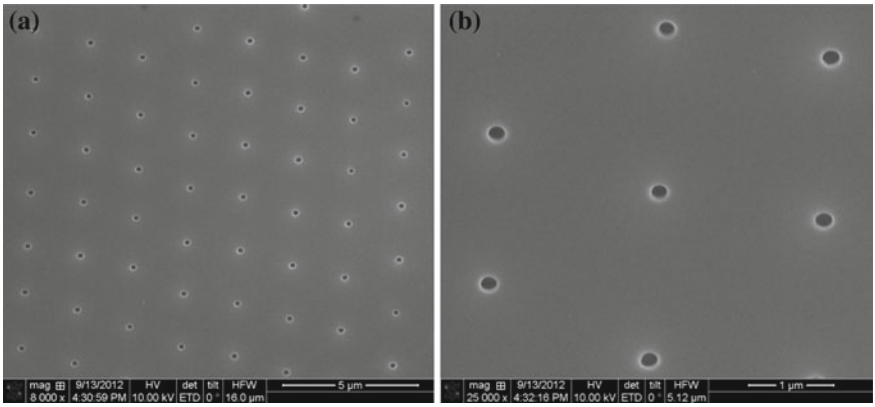

Fig. 1.5 Laser produced voids on a Si-surface buried 10 μm beneath the SiO_2 surface of the oxidised wafer, the SiO_2 was removed using FIB milling, the spacing between the voids is 2 μm: **a** SEM image of FIB-opened section showing an array of voids produced by 170-fs, 800 nm, 300 nJ single laser pulses focused 2 μm apart with ×150 objective; **b** Close-view of (**a**)

Each of the regions irradiated by a single laser pulse at the fluence above ~1 J/cm^2 contains a void located at the focal spot. Figure 1.5 presents arrays of voids at the Si surface produced by 300 nJ single laser pulses focused 2 μm apart with ×150 objective. On the top-view, all the voids had a circular shape and the diameter was 250 nm.

On the area where the SiO_2 layer was not completely removed, cross-section has been obtained using FIB through a void and characterized with SEM. Figure 1.6 shows a side-view of a void produced with an energy of 700 nJ. The maximal horizontal length of the void in the SiO_2 region is 720 nm, in Si 550 nm. The vertical size (including Si and SiO_2) is 1.25 μm. A shock-wave-modified Si surrounded the voids. The thickness of the boundary between the transparent oxidised layer and crystalline Si where the laser radiation is focused is of the order of only 2 nm, it can be clearly seen in electron microscope. Material should be removed from the energy deposition region in order to form a void involving that a denser shell surrounded the void. Therefore the observation of a large void is unequivocal evidence of creation the pressure well in excess the Young modulus of both materials, $Y_{SiO_2} \sim 75$ GPa for SiO_2 and $Y_{Si} \sim 165$ GPa for Si.

The characterization of the laser-affected area, the dense shell surrounding the void and the shock wave affected area by transmission electron microscopy and by Raman micro-spectroscopy will be discuss elsewhere.

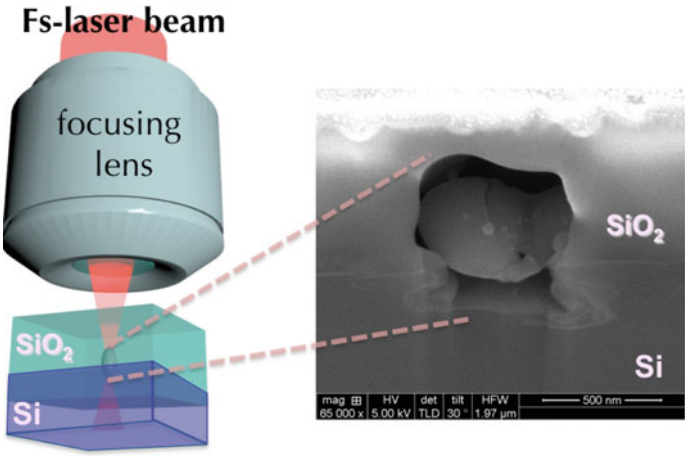

Fig. 1.6 Schematic representation of the laser induced micro-explosion at the Si/SiO2 interface with the associated side-view SEM image of a void produced at the energy of 700 nJ

1.6 Summary

Let us summarise the main conclusions on ultrafast laser-induced material modifications in confined geometry:

- In the conditions close but below the optical breakdown threshold the femtosecond laser pulse creates optically detectable changes in the refractive index. The modifications in refractive index are short-lived and transient. The short-lived modification occurs due to excitation of electrons of all constituent atoms. Permanent modification occurs in the doped sites due to the field of spontaneous polarisation.
- Femtosecond laser pulse tightly focussed by high-*NA* optics leads to absorbed energy density in excess of the strength of any existing material. A void surrounded by a compressed shell is formed as a result of the confined micro-explosion in the focal volume.
- Warm Dense Matter at the pressure exceeding TPa and the temperature more then 100,000 K is created in the table-top experiments, mimicking the conditions in the cores of stars and planets.
- Confined micro-explosion studies open several broad avenues for research, such as formation of three-dimensional structures for applications in photonics, studies of new materials formation, and imitation the inter-planetary conditions at the laboratory tabletop.

It was demonstrated that tight focusing of a conventional tabletop laser inside the bulk of a transparent solid creates pressure exceeding the strength of any material, and the shock wave compresses a solid, which afterwards remains confined inside a crystal. High pressure and temperature are necessary to produce super-dense, super-hard and super-strong phases or materials, which may possess other unusual properties,

such as ionic conductivity. In nature, such conditions are created in the cores of planets and stars. Extreme pressures were recreated by strong explosions, by diamond anvil cell presses and with powerful ns-lasers. All these methods were cumbersome and expensive. By contrast, ultra-short lasers create extreme pressure and temperature along with record high heating and cooling rates by focusing 100–200 nanoJoules of conventional femtosecond laser pulse into a sub-micron volume confined inside a solid [28]. Recently, the crystalline phase of aluminium, bcc-Al has been discovered in ultra-fast laser-induced micro-explosions [29]. These results open the possibilities of formation of new high-pressure phases and prospects of modelling in the laboratory the conditions in the cores of planets and macro-explosions. The first results might be considered a proof-of-principles step. However, it is obvious that, with this simple and inexpensive method for creation of extreme pressure/temperature, the focus in research is shifted to post-mortem diagnosis of shock-compressed material. Micro-Raman, x-ray and electron diffraction, and AFM and STM studies with resolution on the sub-micron level are needed for identification of the new phases. Another challenge is to develop a pump-probe technique with time resolution capable if *in situ* observation of shock-front propagation inside a crystal.

Summing up, the prospects for the fundamental study of ultra-fast laser-matter interaction and its technological applications look extremely encouraging. As the technology becomes smaller, less expensive, more robust, less power-hungry and more energy-efficient, it allows the increased exploitation of ultrafast phenomena, ultimately entering our everyday lives.

Acknowledgments This research was supported under Australian Research Council's Discovery Project funding scheme (project number DP120102980). Partial support to this work by Air Force Office of Scientific Research, USA (FA9550-12-1-0482) is gratefully acknowledged.

References

1. E. Glezer, E. Mazur, Appl. Phys. Lett. **71**, 882–884 (1997)
2. S. Juodkazis, H. Misawa, E. Gamaly, B. Luther-Davies, L. Hallo, P. Nicolai, V.T. Tikhonchuk, Phys. Rev. Lett. **96**, 166101 (2006)
3. S. Juodkazis, H. Misawa, T. Hashimoto, E. Gamaly, B. Luther-Davies, Appl. Phys. Lett. **88**, 1 (2006)
4. E.G. Gamaly, E. G., S. Juodkazis, H. Misawa, B. Luther-Davies L. Hallo, P. Nicolai, V.T. Tikhonchuk, Phys. Rev. B **73**, 214101 (2006)
5. E.G. Gamaly, A.V. Rode, B. Luther-Davies, V.T. Tikhonchuk, Phys. Plasmas **9**, 949–957 (2002)
6. L.D. Landau, E.M. Lifshitz, L.P. Pitaevskii, *Electrodynamics of Continuous Media* (Pergamon Press, Oxford, 1984)
7. D. Arnold, E. Cartier, Phys. Rev. B **46**, 15102–15115 (1992)
8. K. Sokolowski-Tinten, K. J. Bialkowski, A. Cavalieri, M. Boing, H. Schuler, D. von der Linde, in *High-Power Laser Ablation, Proceedings SPIE*, vol. 3343, ed. by C. Phipps, Part 1, 46–57 (1998)
9. B.C. Stuart, M.D. Feit, S. Herman, A.M. Rubenchik, B.W. Shore, M.D. Perry, J. Opt. Soc. Am. B **13**, 459–468 (1996)
10. W. Kautek, J. Krüger, M. Lenzner, S. Sartania, Ch. Spielmann, F. Krausz, Appl. Phys. Lett. **69**, 3146 (1996)

11. M. Lenzner, J. Kruger, S. Sartania, Z. Cheng, Ch. Spielmann, G. Mourou, W. Kautek, F. Krausz, Phys. Rev. Lett. **80**, 4076–4079 (1998)
12. An-Chun Tien, S. Backus, H. Kapteyn, M. Murname, G. Mourou, Phys. Rev. Lett. **82**, 3883–3886 (1999)
13. K. Eidmann, J. Meyer-ter-Vehn, T. Schlegel, S. Huller, Phys. Rev. E **62**, 1202–1214 (2000)
14. YuP Raizer, *Laser-Induced Discharge Phenomena* (Consultant Bureau, New York, 1978)
15. Ya. B. Zel'dovich, Yu. P. Raizer, *Physics of Shock Waves and High-Temperature Hydrodynamic Phenomena* (Dover, New York, 2002)
16. W.L. Kruer, *The Physics of Laser Plasma Interactions* (Addison-Wesley, New-York, 1988)
17. E.G. Gamaly, Phys. Rep. **508**, 91–243 (2011)
18. E. G. Gamaly, L. Rapp, V. Roppo, S. Juodkazis, A. V. Rode, New J. Phys. **15**, 025018 (2013)
19. Sheng-Nian Luo, T. J. Arens, P. D. Asimov, J. Geophys. Res. **108**, 2421 (2003)
20. S. Brygoo, E. Henry, P. Loubeyre, J. Eggert, M. Koenig, B. Loupias, A. Benuzzi-Mounaix, M.R. Le Gloahec, Nat. Mater. **6**, 274–277 (2007)
21. D.G. Hicks, P.M. Celliers, G.W. Collins, J.H. Eggert, S.J. Moon, Phys. Rev. Lett. **91**, 035502 (2003)
22. D. C. Swift, J. A. Hawreliak, D. Braun, A. Kritcher, S. Glenzer, G. Collins, S. D. Rothman, D. Chapman and S. Rose, *in Gigabar material properties experiments on NIF and Omega. Shock Compression of Condense Matter - 2011, AIP Conf. Proc.*, vol. 1426, 477–480 (2012)
23. R.F. Trunin, Physics-Uspekhi **37**, 1123–1146 (1994)
24. E.N. Glezer, M. Milosavjevic, L. Huang, R.J. Finlay, T.-H. Her, J.P. Callan, E. Masur, Opt. Lett. **21**, 2023–2026 (1996)
25. S.A. Akhmanov, V.A. Vyspoukh, A.S. Chirkin, *Optics of Femtosecond Laser Pulses* (Nauka, Moscow, 1988)
26. V.V. Temnov, V. V. K. Sokolowski-Tinten, P. Zhou, A. El-Khamhawy, D. von der Linde, Phys. Rev. Lett. **97**, 237403 (2006)
27. B.C. Stuart, M.D. Feit, A.M. Rubenchick, B.W. Shore, M.D. Perry, Phys. Rev. Lett. **74**, 2248–2251 (1995)
28. E.G. Gamaly, A. Vailionis, V. Mizeikis, W. Yang, A.V. Rode, S. Juodkazis, High Energy Density Phys. **8**, 13–17 (2012)
29. A. Vailionis, E.G. Gamaly, V. Mizeikis, W. Yang, A.V. Rode, S. Juodkazis, Nat. Commun. **2**, 445 (2011)

http://www.springer.com/978-3-319-05986-0

Fundamentals of Laser-Assisted Micro- and Nanotechnologies

Veiko, V.p.; Konov, V.I. (Eds.)

2014, XVII, 322 p. 145 illus., 49 illus. in color., Hardcover
ISBN: 978-3-319-05986-0